A bipolar convection seesaw explains Earth system response to Heinrich events

Matteo Willeit[1*], Andrey Ganopolski[1], Christine Kaufhold[1,2], Daniela Dalmonech[3], Bo Liu[4,6], Tatiana Ilyina[4,5,6]

[1*]Earth System Analysis, Potsdam Institute for Climate Impact Research (PIK), Member of the Leibniz Association, Potsdam, Germany.
[2]Institute of Physics and Astronomy, Universität Potsdam, Potsdam, Germany.
[3]Forest Modelling Laboratory, Institute for Agriculture and Forestry Systems in the Mediterranean, National Research Council of Italy (CNR-ISAFOM), Perugia, Italy.
[4]Universität Hamburg, Hamburg, Germany.
[5]Helmholtz-Zentrum Hereon, Geesthacht, Germany.
[6]Max Planck Institute for Meteorology, Hamburg, Germany.

*Corresponding author(s). E-mail(s): willeit@pik-potsdam.de;
Contributing authors: andrey@pik-potsdam.de; kaufhold@pik-potsdam.de; daniela.dalmonech@cnr.it; bo.liu@uni-hamburg.de; tatiana.ilyina@uni-hamburg.de;

Abstract

Abrupt changes in the Atlantic Meridional Overturning Circulation (AMOC) occurred in the past during Dansgaard-Oeschger and Heinrich events [1, 2], and an AMOC weakening, or possibly even collapse, is projected for the future [3]. The AMOC-driven glacial millennial-scale climate variability is associated with large changes in climate mainly over the North Atlantic region [4, 5], but extending also to the Southern Ocean, where they are particularly pronounced during Stadials featuring Heinrich events [6]. Here we use an Earth system model to show that the qualitative differences between Heinrich Stadials and non-Heinrich Stadials seen in many proxy records can be explained by a sudden start of convection in the Southern Ocean triggered by a collapse of the AMOC induced by large iceberg discharge in the North Atlantic during Heinrich events. The sudden convection onset results in rapid warming and sea ice retreat in the Southern Ocean and the resulting ventilation of the deep ocean explains the rapid CO_2 increase of

~15 ppm on centennial time scales during some Heinrich Stadials seen in ice core records [7, 8]. We propose a general mechanism by which a stop of convection in the North Atlantic triggers convection in the Southern Ocean, in what we call a bipolar convection seesaw, which could also operate following a potential future AMOC collapse.

Keywords: Bipolar convection seesaw, Heinrich events, Dansgaard-Oeschger events, AMOC, Southern Ocean convection

1 Introduction

There is widespread evidence of pronounced AMOC variability during glacial times associated with Dansgaard-Oeschger (DO) and Heinrich (H) events [1, 2, 9–11]. It is now widely accepted that DO events [12] can occur as part of internal variability of the ocean–sea ice–atmosphere system [13] involving spontaneous transitions between weak and strong AMOC modes under certain boundary conditions [14–16], implying alternating cold (Stadial) and warm (Interstadial) conditions in the North Atlantic. Additionally, large discharges of icebergs in the North Atlantic, so-called Heinrich events, originating from instabilities of the Laurentide ice sheet [17–19], occurred repeatedly during glacial times [20–22] and forced a weakening or collapse of the AMOC [11, 23] through the input of large amounts of freshwater into the North Atlantic [24]. Cold stadials containing Heinrich events are referred to as Heinrich Stadials (HSs).

While DO events have a large effect on climate over Greenland [4] and generally at high northern latitudes in the North Atlantic [25], some H events also have a large impact on climate at high latitudes in the Southern Hemisphere [6]. In particular, it has been noted that HSs and non-Heinrich Stadials (nHS), which are almost indistinguishable in Greenland ice core records, have a very distinct imprint on Antarctic climate and atmospheric greenhouse gases. Several proxy records hint at qualitative differences between HSs and nHSs that can not simply be explained by the different amplitude of AMOC perturbations: (i) a large and abrupt CO_2 increase by ~10-15 ppm on centennial time scales during HSs as opposed to a steady decrease of CO_2 during nHSs [7, 8, 26, 27], (ii) a large and abrupt warming of 2-3°C over Antarctica during HSs [6, 28] and (iii) a sudden jump in atmospheric methane concentration during HSs [29]. Various proxies point to a crucial role played by the Southern Ocean (SO) to explain the peculiar dynamics during HSs, in particular through an increased ventilation of the SO [30–34], which is reflected also in the North Atlantic [35]. Several studies have invoked shifts in latitude or changes in intensity of the Southern Hemisphere westerly winds to explain the observed increase in ventilation of the water masses in the SO [8, 36–38], while some suggested enhanced convection and deep water formation to be the cause [33, 34, 39, 40], or a combination of the two processes [41].

However, modelling studies so far have failed to realistically reproduce the timing and amplitude of Antarctic temperature and atmospheric CO_2 variations during HSs or more generally in response to freshwater hosing in the North Atlantic designed to mimic iceberg discharge associated with H events [42–50], except for simulations where convection in the SO was enforced to occur by applying an artificial negative freshwater flux at the surface in the SO [39]. Therefore, a mechanistic understanding of the relation between Northern Hemisphere (NH) and Southern Hemisphere (SH) climate response to AMOC variations remains elusive. Here we use a fast Earth system model with fully interactive carbon cycle to investigate the Earth system evolution during DO and H events and show that deep convection is triggered in the SO as a response to AMOC collapse following H events, explaining the observed large and abrupt Antarctic warming and atmospheric CO_2 increase.

2 Simulated millennial-scale climate variability

We use a fast Earth system model [52, 53] to simulate millennial-scale glacial climate variability (Methods). The model simulates spontaneous DO events under typical mid-glacial conditions [16], with jumps between Stadials and Interstadials being associated with transitions between two different AMOC states [16]. We additionally mimic the effect of a H event iceberg discharge through a prescribed plausible input of freshwater flux into the North Atlantic (Methods) and investigate the Earth system response to combined DO and H events in the model. We run a model simulation with interactive atmospheric CO_2 covering several DO cycles and a H event, with boundary conditions representative for MIS3, including mid-glacial ice sheets, an initial CO_2 of 205 ppm, a CH_4 concentration of 450 ppb, a N_2O concentration of 240 ppb and present-day orbital configuration (Methods).

Our modelling results can be compared to different proxy records for MIS3. The time period around Heinrich Stadial 4 (HS4) has been particularly extensively studied in this respect, with many different high-resolution proxy records available for this period of time. We therefore use it here as a prototype of a succession of DO events and a pronounced HS to compare to our model simulation (Fig. 1).

In terms of temperature the model captures the shape of the response over Greenland, reflecting mainly DO variability associated with transitions in the AMOC state (Fig. 1a,g), even though the amplitude of the temperature change is underestimated in the model [16]. Moving south, the model reproduces very well the sea surface temperature response at the Iberian margin, with the cooling during the HS being as much as three times larger than during nHSs ($\sim$5°C compared to $\sim$1.5°C) (Fig. 1b,h). Over Antarctica, temperatures increase rapidly during the middle of the HS, by $\sim$3-4°C in the model and by $\sim$2-3°C in proxy data, while during nHSs the temperature increase is about a factor 3–5 smaller and happens more gradually during the entire duration of the Stadial (Fig. 1c,i).

The simulated CO_2 response to DO variability is generally within $\sim$5 ppm, in agreement with observations (Fig. 1d,j) and previous modelling results [49]. However, correspondingly to the abrupt warming over Antarctica during the HS, the model simulates a rapid increase in atmospheric CO_2 by $\sim$15 ppm (Fig. 1d,j). This is in good agreement with high-resolution CO_2 ice core record [7, 8], although it seems that the increase recorded in the ice core during HS4 was even more rapid than in the model (Fig. 1d,j). However, ice core data also indicate that the CO_2 increase was more gradual during other HSs [8]. The CO_2 response is partly dampened by the land carbon cycle absorbing part of the CO_2 released by the ocean, and would be markedly larger in the absence of the land response (dashed line in Fig. 1j). The land absorbs carbon through a general increase in primary production due to the CO_2 fertilisation effect induced by the increasing atmospheric CO_2 concentration (Fig. A1f). The increase in CO_2 is accompanied by a ~0.2 permil decrease in $\delta^{13}C - CO_2$, matching ice core data [51] (Fig. 1e,k).

The model also qualitatively reproduces the response of atmospheric CH_4 concentration to DO and H variability (Fig. 1f,l), particularly if the CO_2 fertilisation effect on primary production is disabled (dotted line in Fig. 1l).

Overall, the model reproduces the main features of climate and carbon cycle variability associated with DO and H events, in particular the qualitative differences between HSs and nHSs.

3 Southern Ocean convection during Heinrich Stadials

The simulated millenial-scale climate variability presented above is tightly linked to AMOC variations (Fig. 2a). The Atlantic ocean circulation is fundamentally different during HSs compared to nHSs. The latter are characterized by a substantially weaker AMOC compared to Interstadials (Fig. 2g,h), but with convection still active at several locations in the North Atlantic (Fig. 2d,e), while the large and abrupt freshwater input, which mimics iceberg discharge into the North Atlantic associated with the H event, leads to a rapid stop of convection and eventual shutdown of the AMOC in the model (Fig. 2f,i). Initially, the H event leads to a widespread cooling in the North Atlantic region and only limited localized warming in the South Atlantic (Fig. 3b). However, around 1000 years after the AMOC collapse, widespread convection is suddenly triggered in the SO around Antarctica (Fig. 2b, 2f), following a more gradual convection onset in the Ross Sea (Fig. A2). The abrupt onset of convection has a pronounced impact on climate at high southern latitudes (Fig. 3c), resulting in a large initial warming due to heat released from the deep ocean and consequent large retreat of sea ice (Fig. 2c). The enhanced deep convection in the SO also leads to a strengthening of Antarctic bottom water formation (Fig. 2a,k,l). Convection in the SO then eventually stops after around 500 years as soon as the AMOC starts to recover and convection resumes in the North Atlantic (Fig. 2a,b, Fig. A2).

The abrupt onset of convection has a pronounced impact also on the carbon cycle and different biogeochemical tracers in the ocean (Fig. 3). The SO ventilation increases as a result of both the enhanced convection and the associated sea ice retreat (Fig. 3i). Consequently, the oxygen content of the interior ocean is replenished by the Southern-sourced water (Fig. 3l). Meanwhile, large amounts of carbon that were stored mainly in the deep ocean (Fig. 3o) are brought in contact with the atmosphere, leading to a rapid release of carbon (Fig. 3f) and an atmospheric CO_2 increase of ~15 ppm in a few centuries (Fig. 1j).

Rhodes et al. (2015) [29] suggested that the jump in CH_4 seen in core records during Heinrich Stadial 1 reflects the beginning of the H event, and this argument has been extended also to previous H events [54]. However, our results show that the CH_4 jump in the middle of the HSs rather reflects the timing of the onset of convection in the SO, which is delayed by many centuries relative to the start of the actual H event. In our simulation the CH_4 increase following convection onset in the SO is mainly a consequence of larger emissions from the tropics (Fig. A1i) which is explained by a combination of a general increase in precipitation over SH land (Fig. A1c) and an increase in net primary production due to CO_2 fertilisation (Fig. A1f) with a consequent increase in substrate available for anaerobic microbial decomposition in wetland areas (dotted vs solid lines in Fig. 1l).

The convection process in the SO also induces a large vertical mixing of nutrients that stimulates primary productivity in the ocean (Fig. A1f), as confirmed also by proxy records [36].

Overall, the sudden onset of convection in the SO shown by the model can consistently explain the peculiar temporal dynamics seen in different proxy records during Heinrich Stadials.

4 The bipolar convection seesaw

The term bipolar seesaw has been originally introduced by Broecker (1998) [55], who proposed an anti-phase response of deep sea ventilation in the northern Atlantic and the SO to explain the Antarctic temperature response during the Younger Dryas. Later, Stocker and Johnsen (2003) [56] introduced the *thermal* bipolar seesaw concept to explain the temperature response in Antarctica resulting from changes in the AMOC during glacial times. In their simple and purely thermodynamic model, the changes in meridional heat transport induced by AMOC changes combine with a heat reservoir in the SO to produce the Antarctic temperature response to AMOC perturbations. This simple model has since been widely invoked to explain the relation between Greenland and Antarctic temperature evolution, and even to construct an 800,000-year synthetic record of Greenland temperature variability based on Antarctic ice core data [57]. This concept was further refined based on results of climate model simulations [43] and updated to use Iberian Margin sea surface temperatures instead of Greenland temperatures [58].

However, the thermal seesaw alone can not explain the qualitative differences between nHSs and HSs, particularly the rapid CO_2 rise during the latter and little CO_2 changes during the former. Skinner et al. (2020) [34] suggested that convection in the SO occurred as a response to an AMOC weakening/collapse during HS4 in what they call a bipolar *ventilation* seesaw [59, 60], which amplified Antarctic warming and the atmospheric CO_2 response. However, they do not relate the SO convection directly to the H event and can therefore not explain why convection would occur only during some HSs, but not during nHSs.

Here we propose that to explain the observed millennial-scale glacial climate variability, the bipolar *thermal* seesaw should be complemented by the concept of a bipolar *convective* seesaw. The former operates during the entire DO cycle, while the latter operates only during HSs. Both seesaws operate through the AMOC, but in different ways: the bipolar thermal seesaw operates through the interhemispheric AMOC energy transport, the bipolar convection seesaw operates through a general de-stratification of the ocean caused by the AMOC collapse (Fig. 4) as follows. The reduced northward heat and salt transport in the Atlantic following the AMOC collapse leads to a warming and a salinity pile-up in the upper South Atlantic (Fig. A3b,e), as seen also in other models [43, 61]. The reduced upwelling due to a weaker global overturning circulation following the AMOC collapse causes a general decrease of sub-surface salinity and increase in surface salinity in the ocean (Fig. A3e). At the same time, substantial sub-surface warming occurs (Fig. A3b), but with little changes in sea surface temperatures, which are constrained by negative feedbacks through the atmosphere. As a consequence there is a general increase in surface density due to increased sea surface salinity (Fig. 4b) and a decrease in sub-surface density through a combination of warming and decrease in salinity (Fig. 4a,c, Fig. A3h). This creates an increasingly less stable stratification of the global ocean (Fig. 4d) that eventually leads to convective instability in the SO, the region that is initially closer to neutral density stratification (Fig. 4e). Salinity is the dominant factor in the de-stratification of the SO (Fig. A4).

Convection in the SO is then sustained by an increased southward ocean heat transport in the SO (Fig. A5a,c), caused by the stronger overturning circulation resulting from the enhanced Antarctic deep water formation (Fig. 2l, 3i). While the sea surface is efficiently cooled by the atmosphere, the sub-surface warming resulting from the increased heat transport keeps convection going. As soon as the H event ends, the AMOC slowly starts to recover (Fig. 2a), increasing also the northward ocean heat transport and consequently decreasing the southward heat transport in the SH (Fig. A5c,d) until convection can not be sustained anymore in the SO (Fig. A2). The AMOC recovery is therefore the ultimate cause of the convection stop in the SO. This is confirmed also by additional simulations where the Heinrich event is extended in time, leading to a longer persistence of the AMOC off state (Fig. A6c). Convection in the SO always remains active until the eventual recovery of the AMOC, keeping CO_2 levels and Antarctic temperature high for this whole time period (Fig. A6f,i). The convective bipolar seesaw is thus fully controlled by AMOC dynamics. The quick resumption of the AMOC after the end of the H event is a result of its mono-stability under the considered boundary conditions.

Our model explains why SO convection was triggered only during some HSs, when freshwater input was large enough to cause an AMOC collapse, but not during regular nHSs, during which the AMOC was weak but not in an off state and deep water formation continued, although at a reduced rate, in parts of the North Atlantic.

5 Discussion

We have presented climate model simulations producing deep convection in the SO as a response to H events in the North Atlantic. When a plausible H event is embedded in the internal DO-variability, the model reproduces many of the observed features seen in proxy data for different HSs during the last glacial period, including the exceptionally rapid Antarctic warming and abrupt and large increase in atmospheric CO_2. Our results suggest that understanding of inter-hemispheric interactions associated with glacial climate variability requires a combination of the well-established thermal bipolar seesaw concept, which is well suited for DO variability, and our newly proposed convective bipolar seesaw concept, which is required for the response to H events.

While the general CO_2 and CH_4 increases during HSs are explained by SO CO_2 release and increases in CH_4 emissions from wetlands, both a consequence of the sudden onset of SO convection, CO_2 and CH_4 emissions from substantial increases in biomass burning [62], induced by shifts in precipitation as a response to the start of convection in the SO, could have contributed to the very rapid initial increases and temporary overshoots seen in CO_2 and CH_4 ice core data during some HSs.

A latitudinal shift or change in intensity of the westerlies has been extensively discussed as possible explanation of the peculiar SH climate response during HSs [8, 36–38]. In our model the SH westerlies are instead weakening and shifting slightly southward during HSs (Fig. A7a,b) and a simulation with fixed wind stress shows that changes in the westerlies play a negligible role in the onset of convection in the SO (Fig. A7c,d,e).

Generally, reconstructions indicate that the magnitude of ice discharge during different Heinrich events was potentially quite different [24]. The response in many proxies is large during some HSs, e.g. HS4, HS5 and HS1, but is less apparent during e.g. HS2 and HS3, possibly because these Heinrich events were weaker, and the lower freshwater input did not cause a complete collapse of the AMOC and therefore failed to trigger convection in the SO. This is supported by model simulations where the freshwater hosing is reduced by a factor of two, in which case the AMOC is still substantially weakened, but widespread convection is not triggered in the SO (Fig. A6b,e,h).

The bipolar convection seesaw is a robust feature of our model. It does not depend on the timing of the H event during the DO cycles (Fig. A6a,d,g) and is relatively insensitive to model parameters (Fig. A8). It also works under very different boundary conditions in terms of CO_2 and ice sheets (Fig. A9), but the AMOC becomes more stable with increasing size of the NH ice sheets, meaning that an increasingly larger freshwater flux is needed to collapse the AMOC and trigger convection in the SO.

The robustness of the proposed bipolar convection seesaw with respect to different climate and boundary conditions suggests that it could also operate as a response to a possible future collapse of the AMOC under global warming, with potentially large impacts on regional and global climate and the Antarctic ice sheet. We suggest that Southern Ocean convection should be considered as a tipping element in the Earth system, with the bipolar convection seesaw forming a previously unidentified potential cross-hemispheric link between different tipping elements and more generally connecting ocean circulation, carbon cycle and ice sheets.

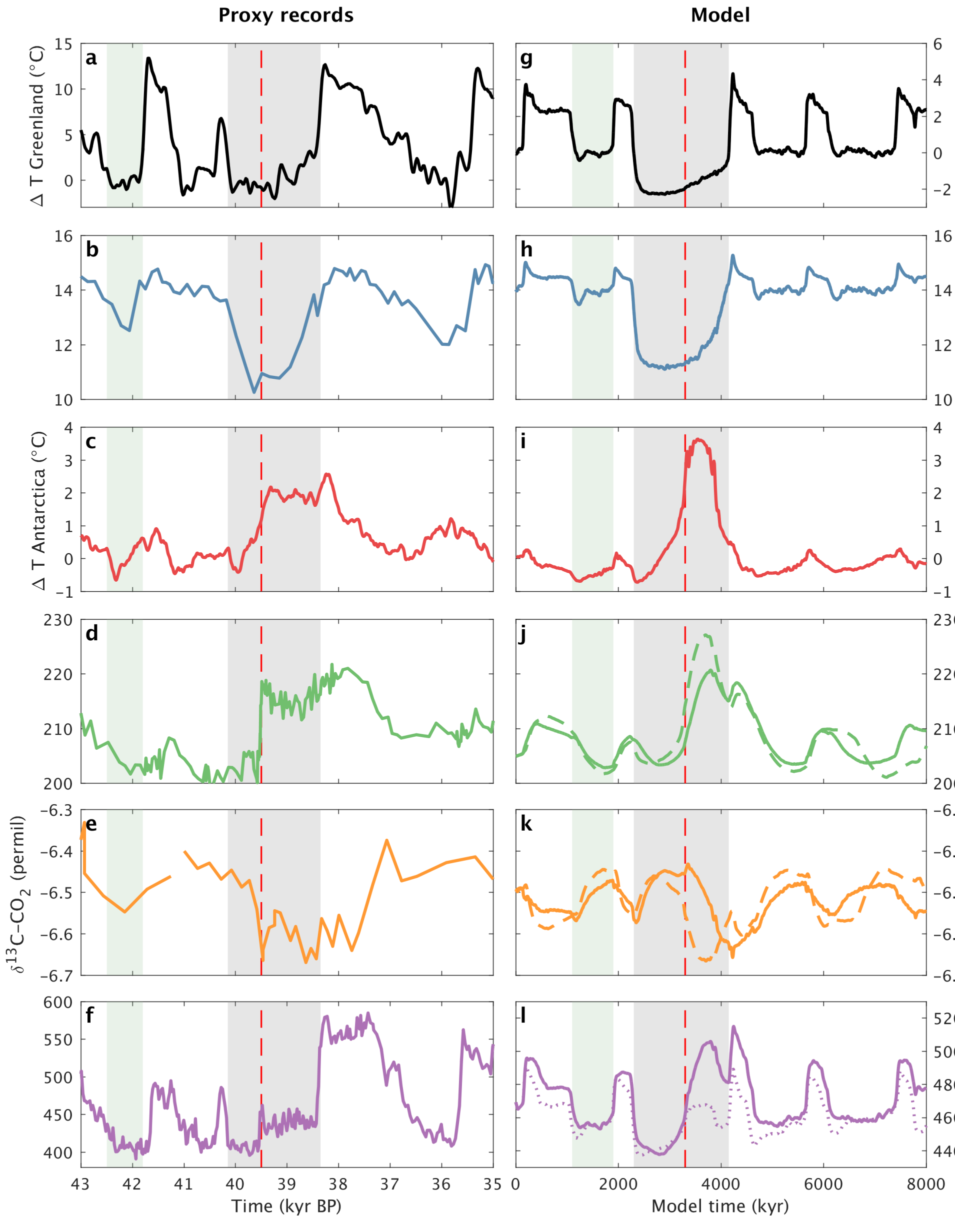

Fig. 1 **Proxy-model comparison of millenial climate variability**. Comparison of simulated climate variability under typical mid-glacial conditions with proxy reconstructions of a time interval around Heinrich Stadial 4. Simulated and reconstructed **a,g** Greenland temperature [4], **b,h** Iberian Margin sea surface temperature [5], **c,i** Antarctic temperature averaged over four ice cores (WDC, EDC, EDML and TALDICE) [28], **d,j** atmospheric CO_2 concentration [7, 8], **e,k** $\delta^{13}C$ of atmospheric CO_2 [51] and **f,l** atmospheric CH_4 concentration [29]. Proxy records are shown in the left column and model simulation results in the right column. The dashed lines in **j,k** show results of a model simulation where the land carbon cycle is not active and only ocean and atmosphere interact to determine atmospheric CO_2. The $\delta^{13}C$ age scale in **e** is shifted by -160 years following ref.[8]. The dotted line in **l** shows CH_4 concentration in a simulation with a prescribed constant CO_2 of 205 ppm and thus represents the simulated CH_4 evolution in the absence of the CO_2 fertilisation effect. The shaded areas indicate the Heinrich Stadial (grey) and a non-Heinrich Stadial (green). The vertical red dashed lines mark the timing of the jump in CH_4 and CO_2 in the left column and the onset of convection in the Southern Ocean in the right column.

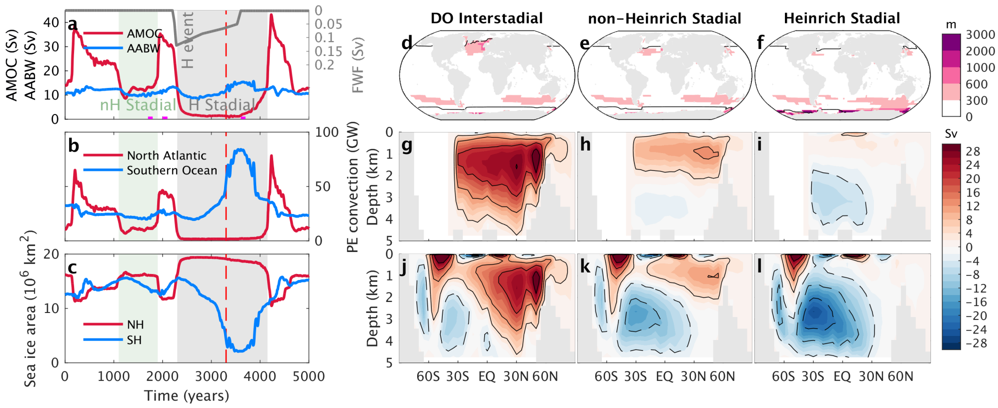

Fig. 2 The bipolar convection seesaw. North Atlantic versus Southern Ocean climate evolution in model simulations for mid-glacial conditions with internally generated DO events and a prescribed Heinrich event. **a**, Time series of the maximum of the Atlantic meridional overturning streamfunction (red), Antarctic bottom water formation rate (blue) and freshwater flux applied to represent a Heinrich event in the North Atlantic (grey). **b**, Time series of the potential energy released by convection in the North Atlantic (north of the Equator) and the Southern Ocean (south of 55°S). **c**, Time evolution of the maximum sea ice area in the two hemispheres. The shaded areas in **a-c** indicate the Heinrich Stadial (HS) and a non-Heinrich Stadial (nHS). **d-f**, Maximum mixed layer depth for three time intervals marked by the magenta intervals in (**a**) representing DO Interstadial (**d**), nHS (**e**) and HS (**f**) conditions. The vertical red dashed lines mark the onset of convection in the Southern Ocean. Black lines indicate the maximum sea ice extent. For the same three time periods the Atlantic (**g-i**) and global (**j-l**) meridional overturning streamfunctions are also shown.

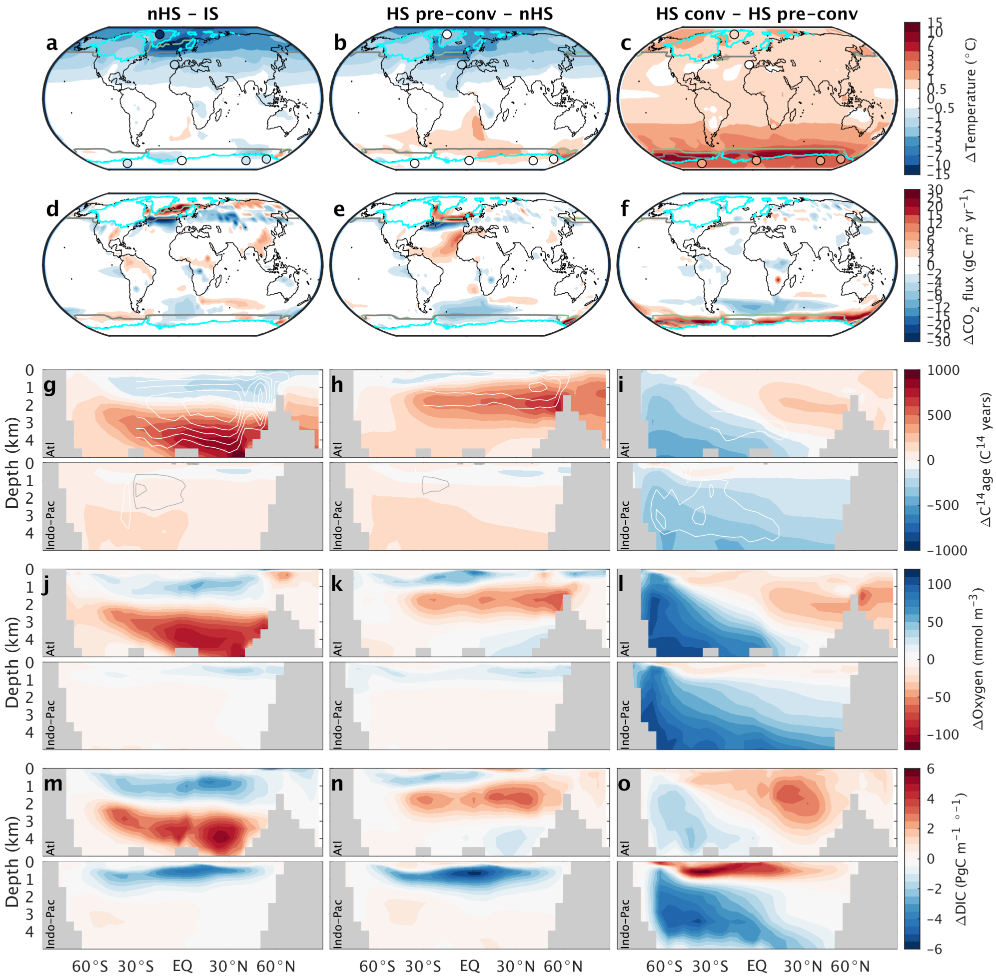

Fig. 3 Climate and ocean biogeochemistry changes during DO and H events. Differences in simulated variables between non-Heinrich Stadial and Interstadial (left), Heinrich Stadial before the onset of convection in the Southern Ocean and non-Heinrich Stadial (middle) and Heinrich Stadial after and before the onset of convection (right) for **a-c** annual mean near-surface air temperature, **d-f** net carbon flux to the atmosphere, **g-i** zonally averaged radiocarbon ventilation age **j-l** zonally averaged oxygen concentration and **m-o** zonally integrated dissolved inorganic carbon content. The filled circles in **a-c** represent temperature changes estimated from proxy records [4, 5, 28]. All ocean fields in **g-o** are shown separately for the Atlantic Ocean and the Indo-Pacific Oceans, with the Southern Ocean sectors being included. The contours in **g-i** indicate changes in the ocean overturning streamfunctions, negative for white contours and positive for grey contours, plotted at intervals of 4 Sv.

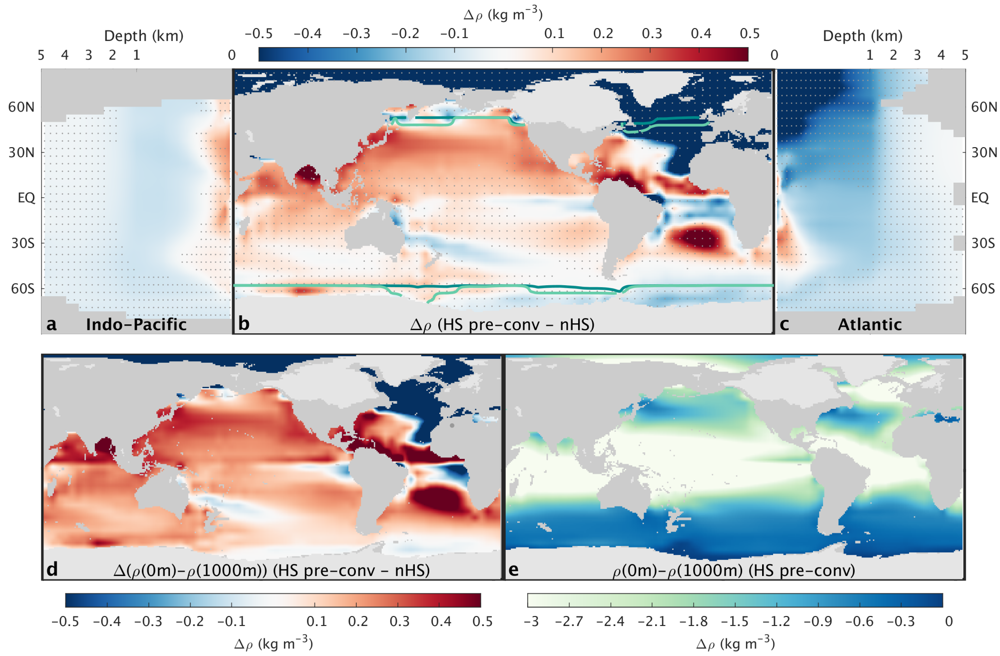

Fig. 4 Bipolar seesaw mechanism. a-c Density differences between the HS prior to the onset of convection in the SO and average nHS conditions at **b** the surface and as zonal average of **a** the Indo-Pacific Oceans and **c** the Atlantic Ocean. The dots indicate regions where the density difference is dominated by changes in salinity, as opposed to temperature changes. The lines in **b** indicate the maximum sea ice extent during the nHS (dark cyan) and the HS prior to convection (green). **d** Change in density difference between the surface and 1000 m depth during the HS prior to convection onset relative to average nHS conditions. **e** Density difference between the surface and 1000 m depth during the HS prior to convection.

6 Methods

6.1 Earth system model

We use the CLIMBER-X Earth system model [52, 53], including the frictional-geostrophic 3D ocean model GOLDSTEIN [63, 64] with 23 vertical layers, the semi-empirical statistical-dynamical atmosphere model SESAM [52], the dynamic-thermodynamic sea ice model SISIM [52], the land surface model with interactive vegetation PALADYN [65] and the ocean biogeochemistry model HAMOCC6 [66–68]. The comprehensive carbon cycle in the model allows to interactively compute the atmospheric CO_2 evolution. Here we employ the 'closed' carbon cycle setup, in which marine sediments and chemical weathering on land are ignored. In this setup carbon is conserved in the atmosphere-ocean-land system, which is a reasonable assumption on millennial scales. All components of the model have a horizontal resolution of $5°\times5°$. Ice sheets are prescribed at their modern state and the net freshwater flux from ice sheets is zero. The model is described in detail in ref. [52] and ref. [53] and in general shows performances that are comparable with state-of-the-art CMIP6 models under different forcings and boundary conditions. Notably, the model has been shown to reproduce DO-like variability under mid-glacial conditions [16] and the stability of the AMOC in the model has been thoroughly explored [69].

6.2 Experiments

The main model experiment is designed to simulate realistic millenial-scale climate variability during glacial times, i.e. Marine Isotope Stage 3. The boundary conditions for this simulation include mid-glacial ice sheets from the GLAC-1D reconstruction [70], a CH_4 concentration of 450 ppb, a N_2O concentration of 240 ppb and present-day orbital parameters. Similarly to ref. [16] we apply noise in the surface freshwater flux in the northern North Atlantic so that the model produces robust internal DO cycles. We first perform a model spinup of 10,000 years with a prescribed atmospheric CO_2 concentration of 205 ppm, to allow the climate and carbon cycle to reach an (oscillating) equilibrium state. Starting from that we then run a 8,000 years long simulation with interactive CO_2. In this simulation we introduce a plausible Heinrich event starting in the year 2200, during a DO Interstadial phase. The prescribed temporal shape of the freshwater flux associated with the Heinrich iceberg discharge event is derived qualitatively using results of different ice sheet model simulations [17, 19, 71], with a peak freshwater flux of 0.13 Sv, followed by a gradual decline until the event ends around 1200 years later (Fig. 2a). Spatially, the freshwater flux is added uniformly to the IRD belt in the North Atlantic, between 40 and 60°N and between 10 and 70°W. No compensation of the freshwater flux is applied and the average ocean salinity decreases by $\sim$0.1 psu by the end of the H event.

In addition to this reference model simulation we have performed a number of simulations to explore the sensitivity of the results to the amplitude (half and double), timing (H event starting at the beginning and in the middle of a Stadial) and duration of the H event (idealized constant 0.1 Sv freshwater flux for 1000, 2000, 3000 and 4000 years).

We also run an ensemble of simulations with perturbed parameters to assess the robustness of the results with respect to changes in ocean model parameters (minimum and maximum diapycnal diffusivities, Gent-McWilliams diffusivity and the maximum slope of the isopycnals). In order to avoid having to run a spinup of the carbon cycle for each of the ensemble members, these experiments are run with a prescribed constant CO_2 of 205 ppm, starting from the same initial condition as the reference run and the H event is applied starting from the year 3000.

To investigate the robustness of our results to changes in boundary conditions, we have performed additional simulations with present-day and last glacial maximum (LGM) ice sheets and with different constant CO_2 concentrations (180, 220 and 280 ppm). These simulations are run for 10,000 years and the H event is applied starting in the year 5000, to give the system enough time to equilibrate with the different boundary conditions. The initial condition for these experiments is a pre-industrial equilibrium state. We have also repeated these simulations with halving and doubling of the amplitude of the H event.

To separate the effect of changes in wind stress over the ocean on the model response to DO and H events, we have run an additional simulation in which the seasonal wind stress fields are kept constant at their initial (non-Heinrich Stadial) state.

To quantify the effect of CO_2 fertilisation on the increase in CH_4 emissions following the onset of SO convection, we have performed an additional simulation with the same boundary conditions as the reference model run, but in which atmospheric CO_2 is prescribed at a constant value of 205 ppm.

Acknowledgements. MW is funded by the German climate modelling project PalMod supported by the German Federal Ministry of Education and Research (BMBF) as a Research for Sustainability initiative (FONA) (grant nos. 01LP1920B, 01LP1917D, 01LP2305B). CK is funded by the Bundesgesellschaft für Endlagerung through the URS project (research project no. STAFuE-21-4-Klei). BL is supported by the German palaeoclimate modelling initiative PalMod (grant number: 01LP2328A). TI is supported by the European Union's Horizon 2020 research and innovation programme (ESM2025 - Earth System Models for the Future - grant no. 101003536), the Deutsche Forschungsgemeinschaft (Germany's Excellence Strategy - EXC 2037 "CLICCS - Climate, Climatic Change, and Society" - project no. 390683824, contribution to the Center for Earth System Research and Sustainability (CEN) of Universität Hamburg), as well as the European Union's Horizon 2020 research and innovation programme 4C (grant no. 821003). The authors gratefully acknowledge the European Regional Development Fund (ERDF), the German Federal Ministry of Education and Research and the Land Brandenburg for supporting this project by providing resources on the high performance computer system at the Potsdam Institute for Climate Impact Research.

Declarations

Competing interests. The authors declare no competing interests.

Data availability. The output of the reference model simulation is available on Zenodo at: https://doi.org/10.5281/zenodo.14710066.

Code availability. The CLIMBER-X model code is available at https://github.com/cxesmc/climber-x. For this study we used the tagged version v1.3.0 of the model.

Author contribution. M.W. and A.G. conceived the study. M.W. designed and performed the model simulations. All authors contributed to the analysis and discussion of the results and the writing of the paper.

Appendix A Extended Data Figures

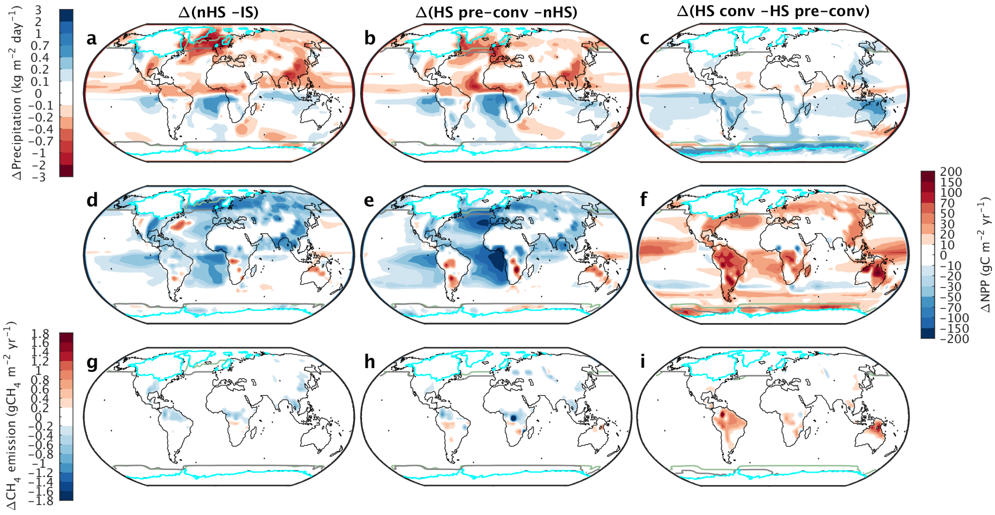

Fig. A1 Changes in precipitation, net primary productivity and CH_4 emissions between different time slices during the DO/H cycles. Same as Fig. 3a-c, but for **a-c** annual precipitation, **d-f** net primary productivity on land and the ocean and **g-i** natural CH_4 emissions from wetlands.

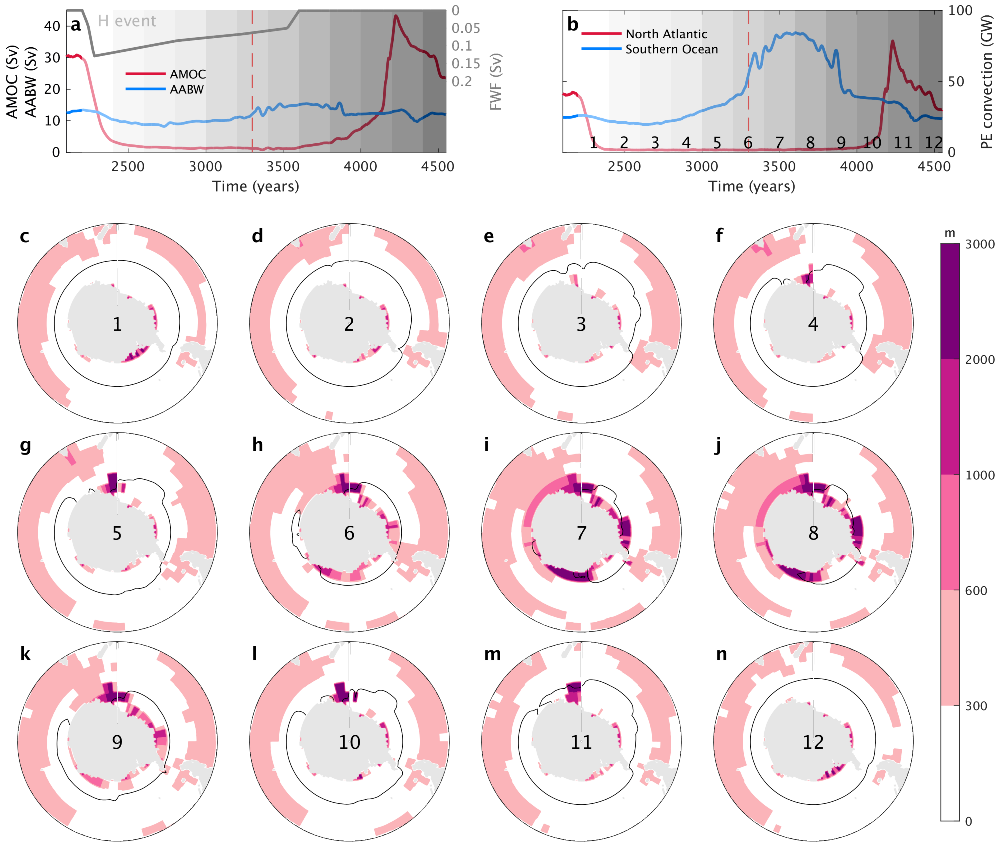

Fig. A2 Evolution of the maximum mixed layer depth in the SO during the HS. c–n Maximum mixed layer depth in the SO at different times during the HS, corresponding to the numbers and shaded grey bars as indicated in **a,b**. Panels **a,b** are the same as those in Fig. 2.

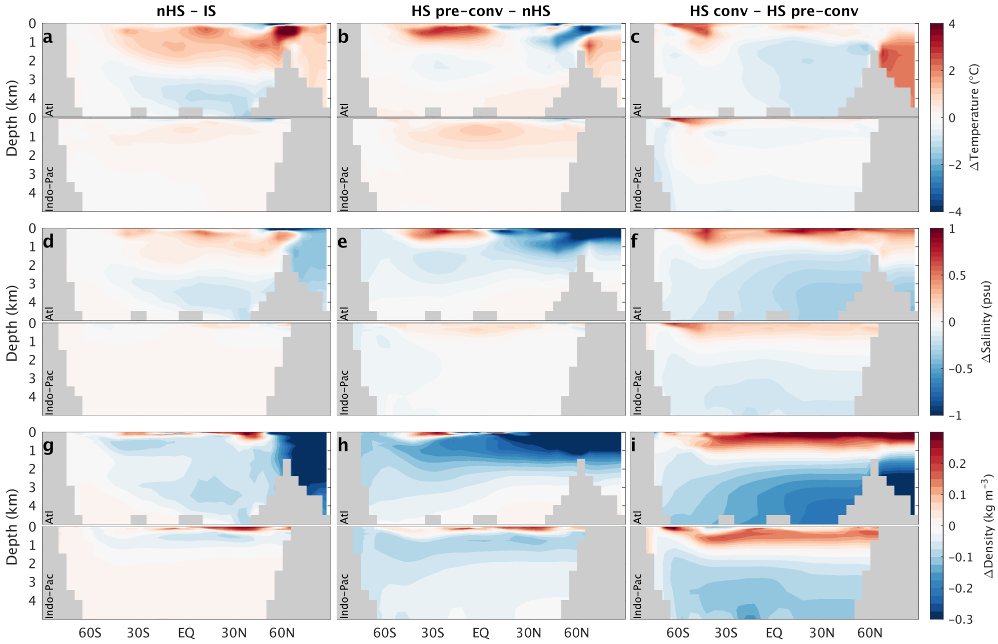

Fig. A3 Changes in ocean temperature, salinity and density. Zonally averaged potential temperature, salinity and density differences between different time periods: (left) nHS relative to Interstadial, (center) HS prior to convection onset in the SO relative to nHS and (right) after convection onset relative to before convection start. All fields are shown separately for the Atlantic Ocean and the Indo-Pacific Oceans, with the Southern Ocean sectors being included.

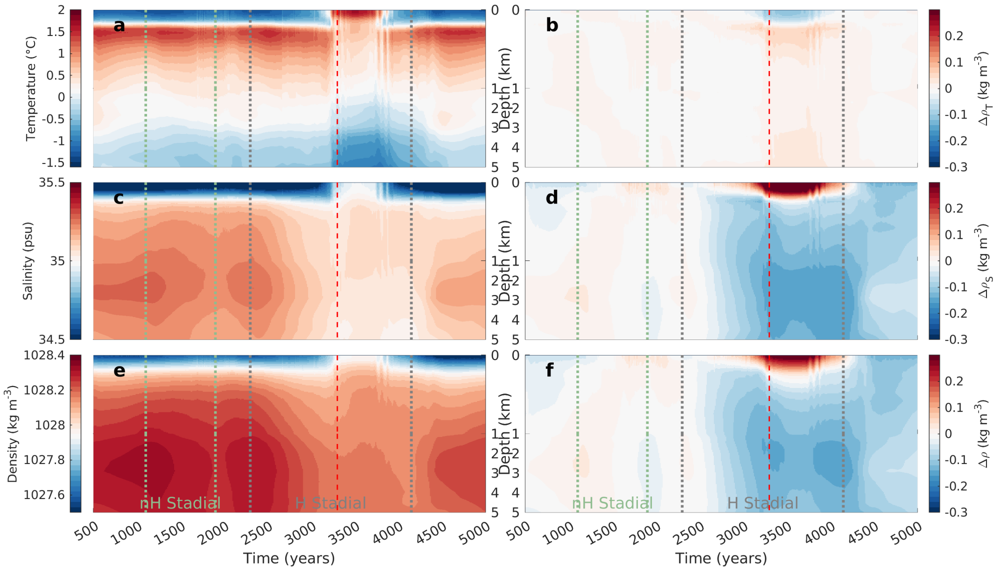

Fig. A4 Ocean temperature, salinity and density evolution in the Southern Ocean. Temporal evolution of vertical profiles of **a** temperature, **c** salinity and **e** density averaged over the Southern Ocean south of 60°S, excluding the Atlantic sector. The right panels show the contributions of **b** temperature and **d** salinity changes relative to average nHS conditions to density changes. The total density changes relative to average nHS conditions are shown in **f**.

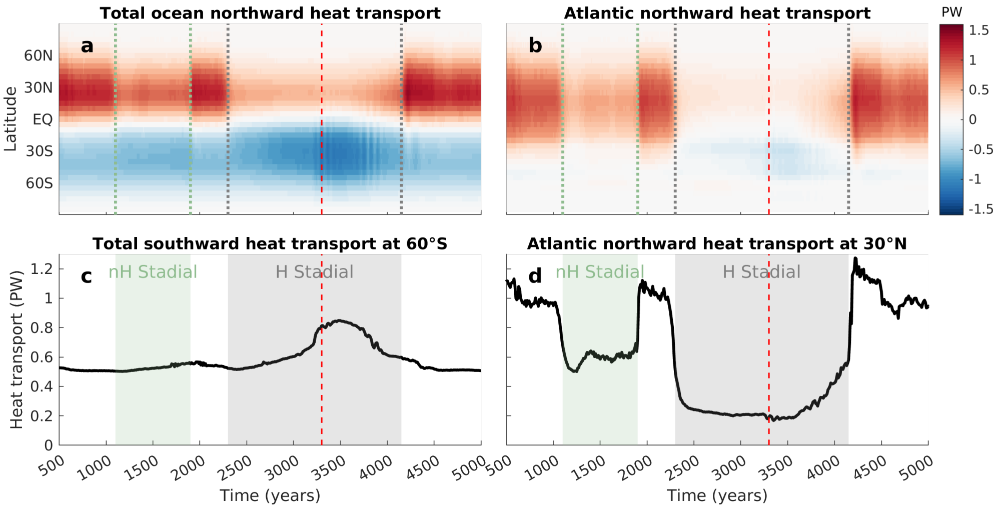

Fig. A5 Evolution of meridional ocean heat transport. **a** Meridional ocean heat transport as a function of time, **b** evolution of the meridional heat transport by the Atlantic over time, **c** evolution of southward ocean heat transport at 60°S and **d** northward heat transport at 30°N in the Atlantic. The timing of the non-Heinrich Stadial and the Heinrich Stadial are marked in the panels and the vertical red dashed line indicates the timing of the onset of convection in the Southern Ocean.

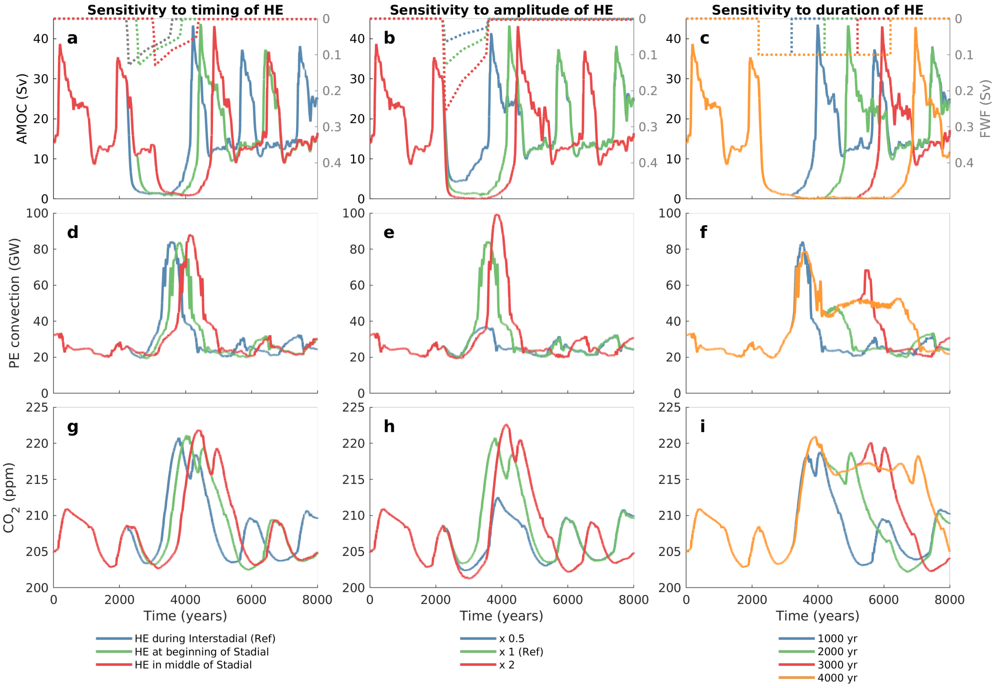

Fig. A6 Sensitivity to timing, amplitude and duration of Heinrich event. Dependence of the simulated AMOC, potential energy released by convection in the Southern Ocean, and atmospheric CO_2 to **a,d,g** the timing, **b,e,h** the amplitude, and **c,f,i** the duration of the Heinrich Event. The dotted lines in the top panels show the freshwater hosing flux applied to the North Atlantic to mimic the different Heinrich events. The legends at the bottom provide the color code for the different lines.

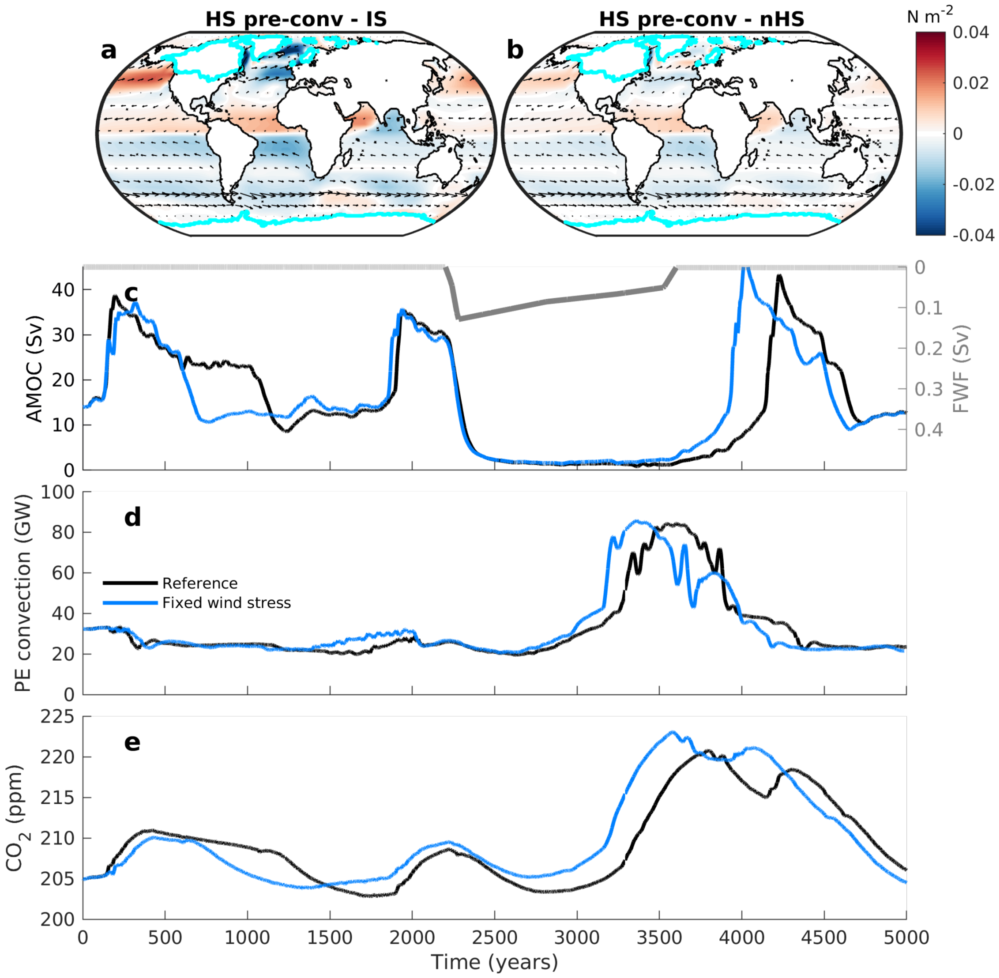

Fig. A7 Sensitivity to wind stress. Changes in simulated wind stress over the ocean between Heinrich Stadial prior to the onset of convection in the Southern Ocean and **a** DO Interstadial and **b** non-Heinrich Stadial. Comparison of simulated evolution of **c** maximum of the Atlantic meridional overturning streamfunction, **d** potential energy released by convection in the Southern Ocean and **e** atmospheric CO_2 in the reference run (black) and in a simulation where the (seasonally varying) wind stress over the ocean is prescribed to average non-Heinrich Stadial conditions (blue).

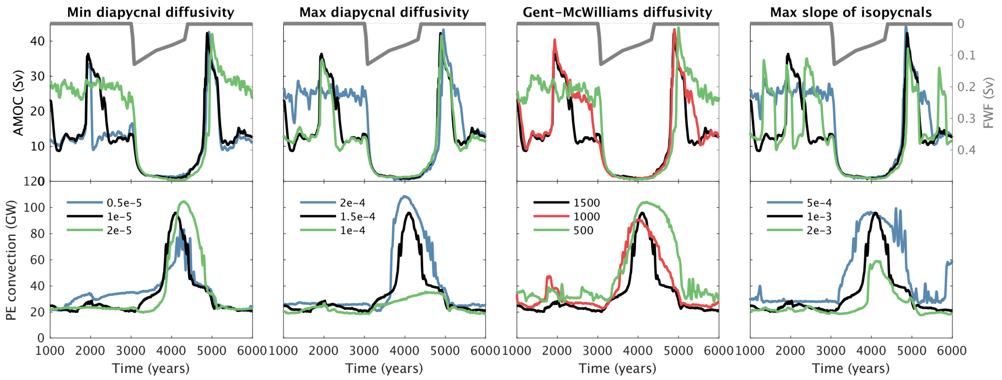

Fig. A8 Sensitivity to ocean model parameters. Dependence of the simulated AMOC and potential energy released by convection in the Southern Ocean to the minimum (surface) value of diapycnal diffusivity (m^2s^{-1}), the maximum (deep ocean) value of diapycnal diffusivity (m^2s^{-1}), the Gent-McWilliams diffusivity (m^2s^{-1}) and the maximum slope of the isopycnals. The values of the parameters used are given in the legends in the bottom panels. All the experiments are for the same boundary conditions corresponding to the reference model simulation presented in the paper.

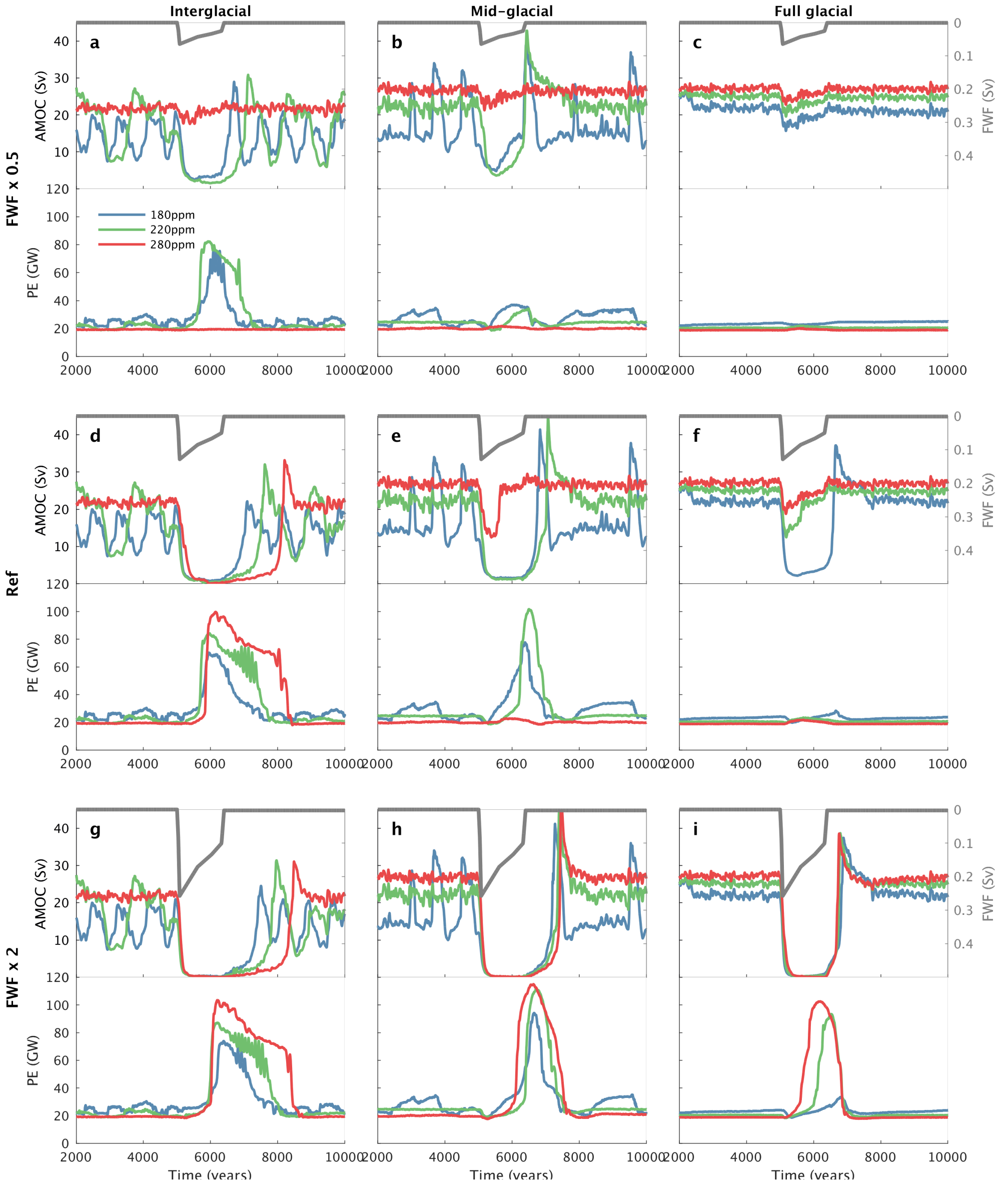

Fig. A9 Sensitivity to ice sheets and baseline atmospheric CO_2 for different amplitudes of the Heinrich event. Maximum of the AMOC streamfunction and potential energy released by convection in the SO for model simulations with interglacial (present-day) ice sheets (left), mid-glacial ice sheets (middle) and full glacial (LGM) ice sheets (right) with different amplitudes of the H event (increasing from top to bottom) and different prescribed constant CO_2 concentrations (180, 220 and 280 ppm) as indicated by the colored lines and the legend.

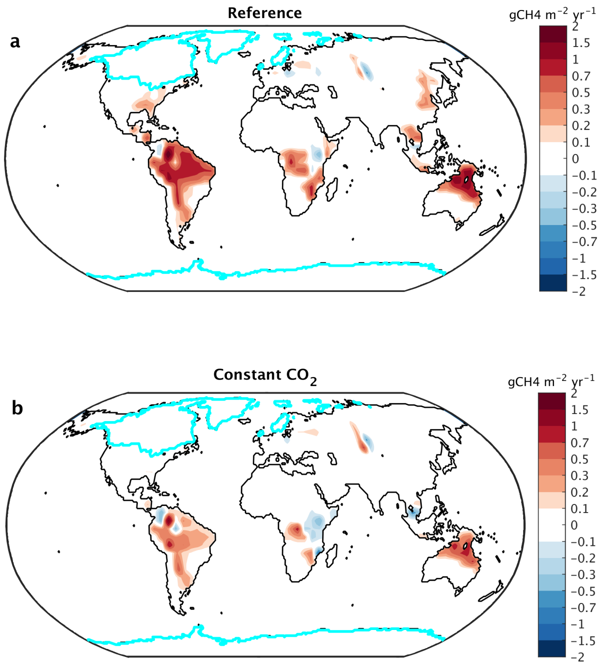

Fig. A10 Changes in CH_4 emissions following SO convection onset. Differences in natural emissions of CH_4 from wetlands between after and before the onset of convection in the SO during the HS in **a** the reference model simulation and **b** an experiment where the CO_2 fertilisation effect is suppressed in the model by prescribing a constant atmospheric CO_2 concentration of 205 ppm in the simulation.

References

[1] Ganopolski, A. & Rahmstorf, S. Rapid changes of glacial climate simulated in a coupled climate model. *Nature* **409**, 153–8 (2001). URL http://www.ncbi.nlm.nih.gov/pubmed/11196631.

[2] Lynch-Stieglitz, J. The Atlantic Meridional Overturning Circulation and Abrupt Climate Change. *Annual Review of Marine Science* **9**, 83–104 (2017).

[3] Weijer, W., Cheng, W., Garuba, O. A., Hu, A. & Nadiga, B. T. CMIP6 Models Predict Significant 21st Century Decline of the Atlantic Meridional Overturning Circulation. *Geophysical Research Letters* **47** (2020).

[4] Kindler, P. *et al.* Temperature reconstruction from 10 to 120 kyr b2k from the NGRIP ice core. *Climate of the Past* **10**, 887–902 (2014).

[5] Martrat, B. *et al.* Four Climate Cycles of Recurring Deep and Surface Water Destabilizations on the Iberian Margin. *Science* **317**, 502–507 (2007). URL https://www.science.org/doi/10.1126/science.1139994.

[6] Jouzel, J. *et al.* Orbital and millennial Antarctic climate variability over the past 800,000 years. *Science (New York, N.Y.)* **317**, 793–796 (2007).

[7] Bauska, T. K., Marcott, S. A. & Brook, E. J. Abrupt changes in the global carbon cycle during the last glacial period. *Nature Geoscience* **14**, 91–96 (2021). URL http://dx.doi.org/10.1038/s41561-020-00680-2.

[8] Wendt, K. A. *et al.* Southern Ocean drives multidecadal atmospheric CO 2 rise during Heinrich Stadials. *Proceedings of the National Academy of Sciences* **121**, 2017 (2024). URL http://www.pnas.org/lookup/suppl/doi:10.1073/pnas.2216830120/-/DCSupplemental.https://doi.org/10.1073/pnas.2216830120https://pnas.org/doi/10.1073/pnas.2319652121.

[9] Rahmstorf, S. Ocean circulation and climate during the past 120,000 years. *Nature* **419**, 207–14 (2002). URL http://www.ncbi.nlm.nih.gov/pubmed/12226675.

[10] Böhm, E. *et al.* Strong and deep Atlantic meridional overturning circulation during the last glacial cycle. *Nature* **517**, 73–76 (2015). URL http://www.nature.com/doifinder/10.1038/nature14059.

[11] Henry, L. G. *et al.* North Atlantic ocean circulation and abrupt climate change during the last glaciation. *Science* **353**, 470–474 (2016).

[12] Dansgaard, W. *et al.* Evidence for general instability of past climate from a 250-kyr ice-core record. *Nature* **364**, 218–220 (1993). URL https://www.nature.com/articles/364218a0.

[13] Menviel, L. C., Skinner, L. C., Tarasov, L. & Tzedakis, P. C. An ice–climate oscillatory framework for Dansgaard–Oeschger cycles. *Nature Reviews Earth and Environment* **1**, 677–693 (2020). URL http://dx.doi.org/10.1038/s43017-020-00106-y.

[14] Peltier, W. R. & Vettoretti, G. Dansgaard-Oeschger oscillations predicted in a comprehensive model of glacial climate: A "kicked" salt oscillator in the Atlantic. *Geophysical Research Letters* **41**, 7306–7313 (2014).

[15] Malmierca-Vallet, I. & Sime, L. C. Dansgaard-Oeschger events in climate models: review and baseline Marine Isotope Stage 3 (MIS3) protocol. *Climate of the Past* **19**, 915–942 (2023).

[16] Willeit, M., Ganopolski, A., Edwards, N. R. & Rahmstorf, S. Surface buoyancy control of millennial-scale variations in the Atlantic meridional ocean circulation. *Climate of the Past* **20**, 2719–2739 (2024). URL https://cp.copernicus.org/articles/20/2719/2024/.

[17] Calov, R., Ganopolski, A., Petoukhov, V., Claussen, M. & Greve, R. Large-scale instabilities of the Laurentide ice sheet simulated in a fully coupled climate-system model. *Geophysical Research Letters* **29**, 1–4 (2002).

[18] Alvarez-Solas, J., Robinson, A., Montoya, M. & Ritz, C. Iceberg discharges of the last glacial period driven by oceanic circulation changes. *Proceedings of the National Academy of Sciences of the United States of America* **110**, 16350–4 (2013). URL http://www.pubmedcentral.nih.gov/articlerender.fcgi?artid=3799353&tool=pmcentrez&rendertype=abstract.

[19] Ziemen, F. A., Kapsch, M.-L., Klockmann, M. & Mikolajewicz, U. Heinrich events show two-stage climate response in transient glacial simulations. *Climate of the Past* **15**, 153–168 (2019). URL https://cp.copernicus.org/preprints/cp-2018-16/cp-2018-16.pdfhttps://cp.copernicus.org/articles/15/153/2019/.

[20] Heinrich, H. Origin and consequences of cyclic ice rafting in the Northeast Atlantic Ocean during the past 130,000 years. *Quaternary Research* **29**, 142–152 (1988).

[21] Bond, G. *et al.* Evidence for massive discharges of icebergs into the North Atlantic ocean during the last glacial period. *Nature* **360**, 245–249 (1992). URL https://www.nature.com/articles/360245a0.

[22] Hemming, S. R. Heinrich events: Massive late Pleistocene detritus layers of the North Atlantic and their global climate imprint. *Reviews of Geophysics* **42** (2004).

[23] McManus, J. F., Francois, R., Gherardi, J.-M., Keigwin, L. D. & Brown-Leger, S. Collapse and rapid resumption of Atlantic meridional circulation linked to deglacial climate changes. *Nature* **428**, 834–7 (2004). URL http://www.ncbi.

nlm.nih.gov/pubmed/15103371.

[24] Zhou, Y. & McManus, J. F. Heinrich event ice discharge and the fate of the Atlantic Meridional Overturning Circulation. *Science* **384**, 983–986 (2024).

[25] Sadatzki, H. *et al.* Sea ice variability in the southern norwegian sea during glacial dansgaard-oeschger climate cycles. *Science Advances* **5**, 1–11 (2019).

[26] Marcott, S. a. *et al.* Centennial-scale changes in the global carbon cycle during the last deglaciation. *Nature* **514**, 616–619 (2014). URL http://www.nature.com/doifinder/10.1038/nature13799.

[27] Nehrbass-Ahles, C. *et al.* Abrupt CO2 release to the atmosphere under glacia and early interglacial climate conditions. *Science* **369**, 1000–1005 (2020).

[28] Markle, B. R. & Steig, E. J. Improving temperature reconstructions from ice-core water-isotope records. *Climate of the Past* **18**, 1321–1368 (2022).

[29] Rhodes, R. H. *et al.* Enhanced tropical methane production in response to iceberg discharge in the North Atlantic. *Science* **348**, 1016–1019 (2015).

[30] Gottschalk, J. *et al.* Biological and physical controls in the Southern Ocean on past millennial-scale atmospheric CO2 changes. *Nature Communications* **7**, 11539 (2016). URL http://www.nature.com/articles/ncomms11539.

[31] Jaccard, S. L., Galbraith, E. D., Martínez-Garciá, A. & Anderson, R. F. Covariation of deep Southern Ocean oxygenation and atmospheric CO2 through the last ice age. *Nature* **530**, 207–210 (2016).

[32] Rae, J. W. *et al.* CO2 storage and release in the deep Southern Ocean on millennial to centennial timescales. *Nature* **562**, 569–573 (2018).

[33] Li, T. *et al.* Rapid shifts in circulation and biogeochemistry of the Southern Ocean during deglacial carbon cycle events. *Science Advances* **6**, 1–10 (2020).

[34] Skinner, L., Menviel, L., Broadfield, L., Gottschalk, J. & Greaves, M. Southern Ocean convection amplified past Antarctic warming and atmospheric CO2 rise during Heinrich Stadial 4. *Communications Earth and Environment* **1**, 1–8 (2020).

[35] Yu, J. *et al.* Millennial atmospheric CO2 changes linked to ocean ventilation modes over past 150,000 years. *Nature Geoscience* **16**, 1166–1173 (2023).

[36] Anderson, R. F. *et al.* Wind-Driven Upwelling in the Southern Ocean and the Deglacial Rise in Atmospheric CO 2. *Science* **323**, 1443–1448 (2009). URL https://www.science.org/doi/10.1126/science.1167441.

[37] Buizert, C. *et al.* Abrupt ice-age shifts in southern westerly winds and Antarctic climate forced from the north. *Nature* **563**, 681–685 (2018). URL http://www.nature.com/articles/s41586-018-0727-5.

[38] Legrain, E. *et al.* Centennial-scale variations in the carbon cycle enhanced by high obliquity. *Nature Geoscience* **17**, 1154–1161 (2024). URL https://www.nature.com/articles/s41561-024-01556-5.

[39] Menviel, L., Spence, P. & England, M. H. Contribution of enhanced Antarctic Bottom Water formation to Antarctic warm events and millennial-scale atmospheric CO2 increase. *Earth and Planetary Science Letters* **413**, 37–50 (2015). URL http://dx.doi.org/10.1016/j.epsl.2014.12.050.

[40] Pedro, J. B. *et al.* Southern Ocean deep convection as a driver of Antarctic warming events. *Geophysical Research Letters* **43**, 2192–2199 (2016).

[41] Menviel, L. *et al.* Southern Hemisphere westerlies as a driver of the early deglacial atmospheric CO2 rise. *Nature Communications* **9**, 1–12 (2018).

[42] Kageyama, M. *et al.* Climatic impacts of fresh water hosing under last glacial Maximum conditions: A multi-model study. *Climate of the Past* **9**, 935–953 (2013).

[43] Pedro, J. B. *et al.* Beyond the bipolar seesaw: Toward a process understanding of interhemispheric coupling. *Quaternary Science Reviews* **192**, 27–46 (2018). URL https://doi.org/10.1016/j.quascirev.2018.05.005.

[44] Schmittner, A. & Galbraith, E. D. Glacial greenhouse-gas fluctuations controlled by ocean circulation changes. *Nature* **456**, 373–376 (2008).

[45] Bouttes, N., Roche, D. M. & Paillard, D. Systematic study of the impact of fresh water fluxes on the glacial carbon cycle. *Climate of the Past* **8**, 589–607 (2012).

[46] Brovkin, V., Ganopolski, A., Archer, D. & Munhoven, G. Glacial CO2 cycle as a succession of key physical and biogeochemical processes. *Climate of the Past* **8**, 251–264 (2012). URL http://www.clim-past.net/8/251/2012/.

[47] Gottschalk, J. *et al.* Mechanisms of millennial-scale atmospheric CO2 change in numerical model simulations. *Quaternary Science Reviews* **220**, 30–74 (2019).

[48] Nielsen, S. B., Jochum, M., Pedro, J. B., Eden, C. & Nuterman, R. Two-Timescale Carbon Cycle Response to an AMOC Collapse. *Paleoceanography and Paleoclimatology* **34**, 511–523 (2019).

[49] Jochum, M. *et al.* Carbon Fluxes during Dansgaard-Oeschger Events as Simulated by an Earth System Model. *Journal of Climate* **35**, 5745–5758 (2022).

[50] Saini, H., Meissner, K. J., Menviel, L. & Kvale, K. Transient Response of Southern Ocean Ecosystems During Heinrich Stadials. *Paleoceanography and Paleoclimatology* **39** (2024). URL https://agupubs.onlinelibrary.wiley.com/doi/10.1029/2023PA004754?af=R&sid=researcher&utm_source=researcher_app&utm_medium=referral&utm_campaign=RESR_MRKT_Researcher_inbound&sid=researcherhttps://agupubs.onlinelibrary.wiley.com/doi/10.1029/2023PA004754.

[51] Bauska, T. K. *et al.* Controls on Millennial-Scale Atmospheric CO2 Variability During the Last Glacial Period. *Geophysical Research Letters* **45**, 7731–7740 (2018).

[52] Willeit, M., Ganopolski, A., Robinson, A. & Edwards, N. R. The Earth system model CLIMBER-X v1.0 – Part 1: Climate model description and validation. *Geoscientific Model Development* **15**, 5905–5948 (2022). URL https://gmd.copernicus.org/articles/15/5905/2022/.

[53] Willeit, M. *et al.* The Earth system model CLIMBER-X v1.0 – Part 2: The global carbon cycle. *Geoscientific Model Development* **16**, 3501–3534 (2023). URL https://doi.org/10.5194/gmd-2022-307https://gmd.copernicus.org/articles/16/3501/2023/.

[54] Martin, K. C. *et al.* Bipolar impact and phasing of Heinrich-type climate variability. *Nature* **617** (2023).

[55] Broecker, W. S. Paleocean circulation during the last deglaciation: A bipolar seesaw? *Paleoceanography* **13**, 119–121 (1998).

[56] Stocker, T. F. & Johnsen, S. J. A minimum thermodynamic model for the bipolar seesaw. *Paleoceanography* **18**, n/a–n/a (2003). URL http://doi.wiley.com/10.1029/2003PA000920.

[57] Barker, S. *et al.* 800,000 Years of abrupt climate variability. *Science* **334**, 347–351 (2011).

[58] Davtian, N. & Bard, E. A new view on abrupt climate changes and the bipolar seesaw based on paleotemperatures from Iberian Margin sediments. *Proceedings of the National Academy of Sciences* **120**, 2017 (2023). URL http://www.pnas.org/lookup/suppl/doi:10.1073/pnas.2216830120/-/DCSupplemental.https://doi.org/10.1073/pnas.2216830120https://pnas.org/doi/10.1073/pnas.2209558120.

[59] Skinner, L. C., Waelbroeck, C., Scrivner, A. E. & Fallon, S. J. Radiocarbon evidence for alternating northern and southern sources of ventilation of the deep Atlantic carbon pool during the last deglaciation. *Proceedings of the National Academy of Sciences of the United States of America* **111**, 5480–5484 (2014).

[60] Skinner, L. *et al.* Rejuvenating the ocean: mean ocean radiocarbon, CO 2 release, and radiocarbon budget closure across the last deglaciation. *Climate of the Past* **19**, 2177–2202 (2023). URL https://doi.org/10.5194/cp-2023-24https://cp.copernicus.org/articles/19/2177/2023/.

[61] Zhu, C. & Liu, Z. Weakening Atlantic overturning circulation causes South Atlantic salinity pile-up. *Nature Climate Change* **10**, 998–1003 (2020). URL http://dx.doi.org/10.1038/s41558-020-0897-7.

[62] Riddell-Young, B. *et al.* Abrupt changes in biomass burning during the last glacial period. *Nature* **637**, 91–96 (2025). URL http://dx.doi.org/10.1038/s41586-024-08363-3.

[63] Edwards, N. R., Willmott, A. J. & Killworth, P. D. On the Role of Topography and Wind Stress on the Stability of the Thermohaline Circulation. *Journal of Physical Oceanography* **28**, 756–778 (1998).

[64] Edwards, N. R. & Marsh, R. Uncertainties due to transport-parameter sensitivity in an efficient 3-D ocean-climate model. *Climate Dynamics* **24**, 415–433 (2005). URL http://link.springer.com/10.1007/s00382-004-0508-8.

[65] Willeit, M. & Ganopolski, A. PALADYN v1.0, a comprehensive land surface–vegetation–carbon cycle model of intermediate complexity. *Geoscientific Model Development* **9**, 3817–3857 (2016). URL http://www.geosci-model-dev-discuss.net/gmd-2016-92/http://www.geosci-model-dev.net/9/3817/2016/.

[66] Ilyina, T. *et al.* Global ocean biogeochemistry model HAMOCC: Model architecture and performance as component of the MPI-Earth system model in different CMIP5 experimental realizations. *Journal of Advances in Modeling Earth Systems* **5**, 287–315 (2013).

[67] Mauritsen, T. *et al.* Developments in the MPI-M Earth System Model version 1.2 (MPI-ESM1.2) and Its Response to Increasing CO2. *Journal of Advances in Modeling Earth Systems* **11**, 998–1038 (2019).

[68] Liu, B., Six, K. D. & Ilyina, T. Incorporating the stable carbon isotope 13C in the ocean biogeochemical component of the Max Planck Institute Earth System Model. *Biogeosciences* **18**, 4389–4429 (2021).

[69] Willeit, M. & Ganopolski, A. Generalized stability landscape of the Atlantic meridional overturning circulation. *Earth System Dynamics* **15**, 1417–1434 (2024). URL https://esd.copernicus.org/articles/15/1417/2024/.

[70] Tarasov, L., Dyke, A. S., Neal, R. M. & Peltier, W. R. A data-calibrated distribution of deglacial chronologies for the North American ice complex from glaciological modeling. *Earth and Planetary Science Letters* **315-316**, 30–40 (2012).

URL http://www.sciencedirect.com/science/article/pii/S0012821X11005243.

[71] Schannwell, C., Mikolajewicz, U., Ziemen, F. & Kapsch, M.-l. Sensitivity of Heinrich-type ice-sheet surge characteristics to boundary forcing perturbations. *Climate of the Past* **19**, 179–198 (2023). URL https://cp.copernicus.org/articles/19/179/2023/.